Off-Resonant Optical Excitation of Gold Nanorods: Nanoscale Imprint of Polarization Surface Charge Distribution

ARTICLE *in* JOURNAL OF PHYSICAL CHEMISTRY LETTERS · DECEMBER 2010

Impact Factor: 7.46 · DOI: 10.1021/jz1014696

9 AUTHORS, INCLUDING:

Prashant K Jain
University of Illinois, Urbana-Champaign
63 PUBLICATIONS **9,020** CITATIONS
SEE PROFILE

Jérôme Plain
Université de Technologie de Troyes
123 PUBLICATIONS **1,168** CITATIONS
SEE PROFILE

Olivier Soppera
French National Centre for Scientific Research
183 PUBLICATIONS **1,047** CITATIONS
SEE PROFILE

THE JOURNAL OF PHYSICAL CHEMISTRY Letters

pubs.acs.org/JPCL

Off-Resonant Optical Excitation of Gold Nanorods: Nanoscale Imprint of Polarization Surface Charge Distribution

Claire Deeb,[†] Xuan Zhou,[†] Davy Gérard,[†] Alexandre Bouhelier,[‡] Prashant K. Jain,[§] Jérôme Plain,[†] Olivier Soppera,[⊥] Pascal Royer,[†] and Renaud Bachelot*,[†]

[†]Laboratoire de Nanotechnologie et d'Instrumentation Optique LNIO-ICD, Université de Technologie de Troyes, France, [‡]Laboratoire Interdisciplinaire Carnot de Bourgogne CNRS-UMR 5209, Université de Bourgogne, Dijon, France, [§]Miller Institute for Basic Research in Science and Department of Chemistry, University of California, Berkeley, California 94720, United States, and [⊥]Institut de Science des Matériaux de Mulhouse IS2M-CNRS LCR 7228, Université de Haute-Alsace, Mulhouse, France

ABSTRACT We report on the nanoscale optical characterization of gold nanorods irradiated out of their plasmonic resonance. Our approach is based on the reticulation of a photopolymerizable formulation locally triggered by enhanced electromagnetic fields. The tiny local field enhancement stems from the surface polarization charges associated with the electric field discontinuity at the metal/dielectric interface. This allows us to get a nanoscale signature of the spatial distribution of the surface charge density in metallic nanoparticles irradiated off-resonance.

SECTION Nanoparticles and Nanostructures

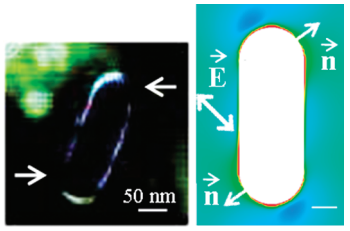

It is a classical exercise for a student in electromagnetism to study the behavior of an electric field at the interface between a metal and a dielectric medium. This situation is a simple application case of the boundary conditions for the electromagnetic fields; the discontinuity of the normal component of the electric field vector at the interface is related to a surface charge density ρ.[1] From the same configuration (i.e., a metal/dielectric interface), it is possible to derive the existence condition of a surface wave propagating along the interface. This surface wave, known as a surface plasmon, is associated with the collective oscillation of the surface charges and is a resonant phenomenon. Surface plasmons are currently the focus of strong interest in the physical chemistry community[2−5] due to their appealing properties for solar energy harvesting,[6] optical manipulation,[7] efficient light generation,[8−10] nanoscale light guiding,[11] and nanosensing.[12] The difference between the resonant (surface plasmon) and off-resonant cases can be understood as follows. Away from the resonance, we are essentially in a quasi-static situation, with the charges oscillating in time at the exciting field frequency (AC field). At resonance, there is a wave propagating along the interface, the so-called surface plasmon wave, meaning that electrons are oscillating both in time and space along the interface. In the case of metallic nanoparticles, different surface plasmon resonances may exist; each one corresponds to a given mode of the electromagnetic field, with its own associated field distribution. The intensity of the associated field can be orders of magnitude higher than the incident field due to the resonant nature of the phenomenon. In the off-resonance case, there is still an associated field localized at the interface, but its amplitude is dramatically lower than that in the resonant case. A remarkable exception is the so-called lightning rod effect,[13] which arises from geometrical singularities; near a sharp protrusion on a metallic surface, the electric field reaches high intensity values. This effect has been experimentally observed in the case of metal nanorods and tips.[14,15] It is very polarization-dependent, and this dependence is related to the above-evoked field boundary conditions. Apart from the lightning rod effect that benefits from charge density enhancement at singularities,[15,16] only few experimental reports on nonresonant effects have been reported[17,18] because off-resonant excitation generates weak fields that are extremely difficult to measure.

In this Letter, we report on imaging of the nonresonant field on a metal/dielectric interface on gold nanorods. Our approach relies on the use of a photopolymer that undergoes photo-cross-linking to embody the profile of the electric field intensity. This photochemical approach has already been employed to image the resonant behavior of metallic nanoparticles (i.e., their surface plasmon resonance).[19,20] We show here that the sensitivity of the photopolymer is high enough to imprint the local nonresonant field with nanoscale resolution, thus allowing what we believe to be the first visualization of the surface charge density distribution.

Gold nanorods (GNRs) were fabricated on a glass substrate by electron beam lithography and lift-off techniques. The structures are differently oriented with respect to the vertical

Received Date: October 29, 2010
Accepted Date: December 7, 2010
Published on Web Date: December 10, 2010

DOI: 10.1021/jz1014696 | *J. Phys. Chem. Lett.* **2011**, *2*, 7–11

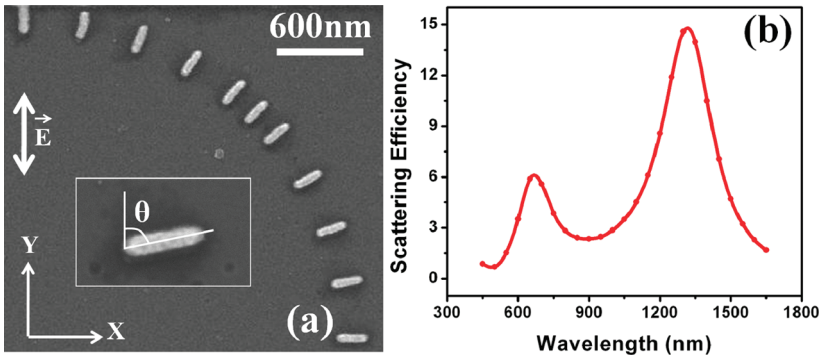

Figure 1. (a) Representative scanning electron micrographs (SEM) showing 11 differently oriented GNRs. The incident field polarization direction is represented by the double white arrow. The inset of panel (a) shows the angle θ between the nanorod major axis and the polarization direction. (b) Calculated far-field scattering spectrum for a single rod, embedded in a medium of refractive index 1.485, corresponding to that of the photopolymerizable solution, illustrating the localized surface plasmon response of both nanorod axes.

direction, alternating from $\theta = 0°$ (for which the major axis of the rod is parallel to the Y in-plane axis) to $\theta = 90°$ (for which the major axis is perpendicular to the Y axis), as illustrated in Figure 1a. We will show that this configuration allows for studies of the influence of the incident polarization. The nanorod length and width are respectively 235 and 85 nm, with a thickness of 28 nm. The corresponding far-field scattering spectrum was calculated using the discrete dipole approximation method (DDA)[21] for a single gold nanorod in an effective medium with a refractive index of 1.5, corresponding to a nanorod on a glass substrate ($n = 1.5$) and embedded in the photosensitive solution ($n = 1.48$). Nanorod dimensions were chosen to be equal to those measured experimentally using atomic force microscopy (AFM). The DDA simulations were performed using DDSCAT 7.0 with a tolerance of 1×10^{-5}. The target was defined by a cubic lattice of virtual dipoles with a mesh spacing of 2 nm. The dielectric function of gold was described by the experimental data for bulk from Johnson and Christy without any additional size correction. The spectrum reveals the minor and major axes surface plasmon responses, which are located at around 662 and 1313 nm, respectively, and is illustrated on Figure 1b.

Our approach relies on a nanoscale photopolymerization induced by the local field intensity in the vicinity of GNRs.[19,20] After morphological characterization using AFM, the GNRs are coated with a photopolymerizable formulation drop and illuminated out of their resonance, at a wavelength of $\lambda = 530$ nm that matches the maximum of the photopolymerizable formulation absorption spectrum but is sufficiently off-resonant from the nanorod surface plasmon responses. Preliminary spectral studies performed in air in the visible region showed a resonance peak corresponding to the minor axis mode at 680 nm, which is close to the DDA value except for a small red shift. This guarantees that we are off-resonance when illuminating at 530 nm.

The optical exposure is performed under normal incidence (having an incident wave vector perpendicular to the XY sample plane) with a 1 cm wide Gaussian laser beam from an Ar/Kr laser source and is linearly polarized along the Y axis. The visible-sensitive free radical photopolymer solution exhibits a threshold dose below which no polymerization can occur.[19,20] The exposure dose is chosen to be smaller than the threshold dose to guarantee that no chain reaction is initiated by the far-field incident laser beam. Here, the exposure dose was chosen to be 65% of the threshold dose to avoid any far-field photopolymerization. However, the threshold dose might be overcome by any local field enhancement originating from the GNRs. In such a case, the polymerization chain reaction is initiated, leading to reticulation. The polymerized parts are then revealed by a rinsing procedure which consists of removing any nonreticulated monomer. Finally, AFM characterization is carried out and compared to AFM images obtained on the same GNRs before the photopolymerization procedure. Such a differential imaging approach accurately depicts the spatial distribution of the polymerization resulting from the reticulation process while circumventing the apparent increase of the polymer depth due to convolution with the AFM tip. The overall resolution of this technique is better than 5 nm,[20] meaning that it is able to imprint enhanced fields localized within regions smaller than 5 nm.

The procedure was performed on several samples, each sample consisting of 11 differently oriented GNRs similar to those shown in Figure 1a. Figure 2 shows typical AFM images for three different values of θ, 0 (Figure 2a), 22.5 (Figure 2b), and 90° (Figure 2c). For each single orientation, we present an AFM image before the procedure (first column in Figure 2), after photopolymerization and rinsing (second column), and a differential image (third column). It is clear from the differential AFM images that a very localized polymerization occurs at the GNR surface, whose extension and geometry depend on the relative orientation of the rod with respect to the incident polarization direction. The polymer extension is maximum when the unit vector normal to the GNR surface $\vec{n}$ is aligned with the polarization direction, as can be seen, for example, at the ends of the GNR in Figure $2a_2$ and at the GNR sides in Figure $2c_2$. Conversely, the polymer extension is null when $\vec{n}$ is perpendicular to the polarization, as one can see at most of the GNR sides in Figure $2a_2$ and at the GNR ends in Figure $2c_2$. In the case of the inclined rod, it is quite remarkable that only two regions on the surface show no polymer extension, as pointed out by the two white arrows in Figure $2b_2$. These specific surface regions present a local unit normal vector $\vec{n}$ that is perpendicular to the incident polarization, while in all other regions, the incident field has a nonzero

DOI: 10.1021/jz1014696 | J. Phys. Chem. Lett. 2011, 2, 7–11

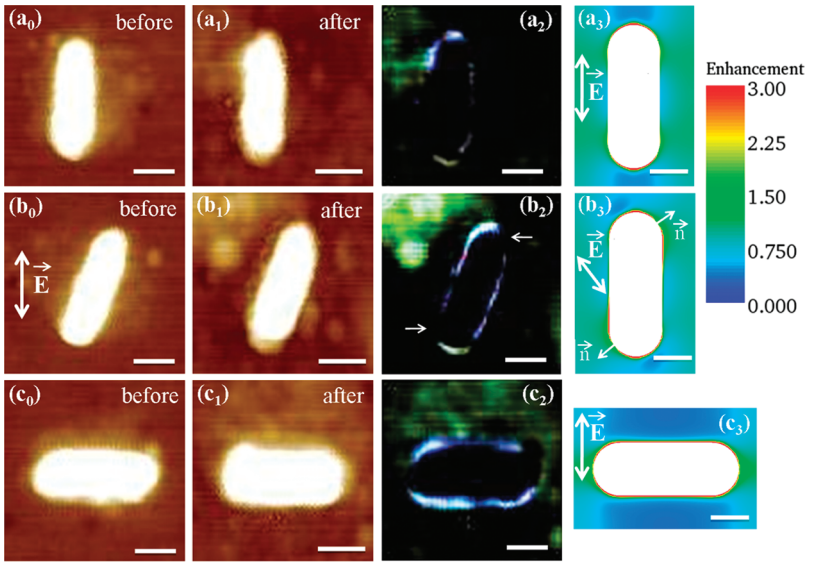

Figure 2. Highlighting the elongation of the minor and the major axes of the nanorod. The three rows of this figure illustrate three GNRs oriented differently with respect to the incident polarization, $\theta = 0$, 22.5, and 90°. (a_0−c_0) AFM images of GNRs before the procedure. (a−c_1) AFM images after the procedure. (a_2−c_2) Differential images that result from the subtraction between the first and the second columns. (a_3−c_3) Near-field calculations performed using FDTD on a GNR, embedded in a medium with a refractive index of 1.485, for differently oriented incident polarization indicated by the white double-headed arrow. The scale bars in all panels represent 90 nm.

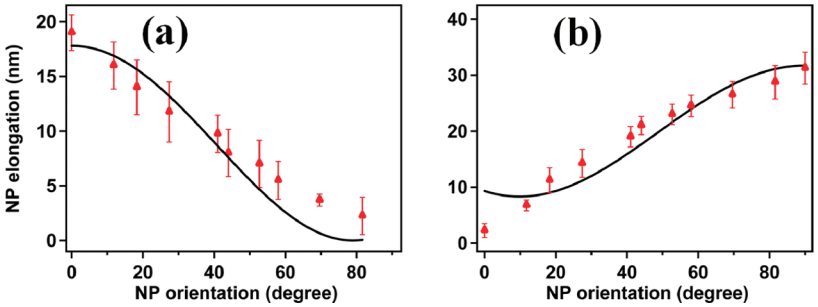

Figure 3. Dependence of the nanoparticle elongation on its orientation with respect to the Y axis. (a) Red triangles: Experimental major axis elongation of GNRs (averaged from several samples). Black solid line: fit by $l = l_0(1 + \chi^2 \cos^2\theta + 2\chi \cos\theta)$, with $\chi = -5.2 \pm 0.1$. (b) Same for the minor axis with $l = l_0(1 + \chi^2 \sin^2\theta + 2\chi \sin\theta) + l_1$ as a fit function, where $\chi = -5.8 \pm 0.3$ and $l_1 = 8.3$ nm. The error bars of the red triangles represent the standard experimental deviation.

projection on $\vec{n}$. This implies that any drastic change in the direction of the normal vector with respect to the incident field that can result from an imperfection during the e-beam procedure or to an impurity on the GNR surface is emphasized by our approach.

We propose that the local polymerization is driven by the excited surface charges related to the electric field discontinuity at the rod interface, following the usual boundary condition, $E_{1n} - E_{2n} = (\rho_{s,pol}/\varepsilon_0) = \chi n \cdot \vec{E}_0$, where E_{1n} and E_{2n} are the normal components of the electric field inside and outside of the rod, respectively, E_0 is the incident electric field, $\rho_{s,pol}$ is the surface density of polarization charges, and χ is the metal electric susceptibility. In turns, the excited surface charges create their own electric field which is responsible for a weak field enhancement on the rod surface and subsequent polymerization. In the following, we present the rationale for our proposal, on the basis of two different arguments.

First, we present in Figure 3 the observed GNR elongation l along its major and minor axes as a function of θ, its orientation with respect to the incident field polarization (Y axis direction; see Figures 1a and 2b_0). Along the major axis (red triangles in Figure 3a), the elongation is maximum for $\theta = 0$, namely, a rod aligned with the polarization direction, and decreases as the rod is tilted, reaching 0 (no polymerization) when the rod is perpendicular to the polarization direction ($\theta = 90°$). Conversely, along the minor axis (red triangles in Figure 3b), the elongation is maximum when $\theta = 90°$. To understand this behavior, a phenomelogical model can be developed.

Above the threshold, the polymer extension is roughly proportional to the field intensity at the rod surface I_{surf}, that is, $l = \alpha I_{surf}$, where α is a parameter depending on the photophysical properties of the polymer and I_{surf} corresponds to the surface field intensity. The electric field at the GNR surface is the sum of the incident field E_0 and the field $\chi n \cdot \vec{E}_0$ created by

DOI: 10.1021/jz1014696 | J. Phys. Chem. Lett. 2011, 2, 7–11

the surface charges. Summing the fields coherently and projecting them along both GNRs axes yields the following intensity expressions, $I_{surf}^{M} = I_0(1 + \chi^2 \cos^2\theta + 2\chi \cos\theta \times \cos\Phi)$ and $I_{surf}^{m} = I_0(1 + \chi^2 \sin^2\theta + 2\chi \sin\theta \times \cos\Phi)$, respectively, where M and m stand, respectively, for the major and the minor axes and Φ is the phase difference between the incident field and the induced dipole field. On the basis of this model and assuming the field scattered by the dipoles constituting the GNRs to be in phase with the incident field, we have fitted the experimental elongation along the major axis by $l = l_0(1 + \chi^2 \cos^2\theta + 2\chi \cos\theta)$ (black line in Figure 3a), where χ is the only fitting parameter. The $l_0 = \alpha \times I_0$ was set to be equal to 1 nm, representing the minimum elongation that can be detected using AFM (corresponding to the AFM lateral resolution). The agreement is good, and we obtain $\chi = -5.2 \pm 0.1$. Along the minor axis, the fit function was chosen as $l = l_0(1 + \chi^2 \sin^2\theta + 2\chi \sin\theta) + l_1$, where l_1 is an offset. The coefficient l_0 was set at the same value of that in the case of the major axis because the incident intensity is the same along both axes. We found $\chi = -5.8 \pm 0.3$ and $l_1 = 8.3$ nm. Again, good agreement is observed between the fit and the experimental data. The origin of the offset is explained as follows. Along the minor axis, the GNR surface in contact with the photopolymerizable solution, namely, the nanorod sides, is much greater than the surface of contact along the major axis, which is limited to the rod ends. This induces a higher probability of adhesion of the formulation on the rod sides, and a tiny layer of polymer may remain attached to the GNR sides after the rinsing procedure, even in the absence of photoexcitation. This is why we observe a 3 nm elongation of the minor axis at $\theta = 0°$. It is worth noticing that equivalent values for χ were found for both axes. From the susceptibility, we can deduce the real part of the dielectric constant of gold because $\varepsilon_r = 1 + \chi$. Averaging both axes, we obtain $\varepsilon_r = -4.5$, in notable agreement with reported values for gold at $\lambda = 530$ nm.[22] This model constitutes the first evidence that the polymer elongation is directly related to surface charges created on the GNR through gold susceptibility and permittivity.

To confirm our proposal, we performed numerical simulations to compute the near-field enhancement at the GNR surface. Calculations were performed using the three-dimensional finite difference time domain (3D-FDTD) method[23] in which GNRs were illuminated by a plane wave at 530 nm and a propagative wave vector along the nanorod thickness. Field intensity values were normalized by those from a blank run without a GNR in order to obtain the field intensity enhancement. Results are summarized in the fourth column of Figure 2 for three values of θ corresponding to experimental values. The computed near-field maps exhibit a striking qualitative agreement with the experimental results shown in column three of Figure 2.

For the $\theta = 0°$ case shown in Figure $2a_2$, no polymerization is observed on the two side surfaces of the nanorod, where the surface-normal unit vector $\vec{n}$ is perpendicular to the incident polarization direction $\vec{E}$. On the other hand, for $\theta = 90°$ (Figure $2c_2$), no polymerization is seen at the two ends of the nanorod, in which case too, $\vec{n}$ is perpendicular to $\vec{E}$. The $\theta = 22.5°$ case (Figure $2b_2$) is particularly instructive, where it is worth highlighting that no polymerization was experimentally observed at two precise regions on the GNR surface (white arrows in Figure $2b_2$), exactly where $\vec{n}$ is perpendicular to $\vec{E}$. These observations are attributed to the fact that no surface charges are excited at locations where the unit normal $\vec{n}$ is perpendicular to the incident field direction, resulting in the enhancement factor at these locations being insufficient to overcome the threshold dose for polymerization. The field enhancement distributions obtained from FDTD clearly reflect this. For each of the polarization directions (Figure $2a_3$, b_3, and c_3), at all of the locations on the GNR where $\vec{n}$ is perpendicular to $\vec{E}$, the field enhancement is significantly lower than the maximum field enhancement on the GNR surface.

It is worth emphasizing that local heating of the nanorod may create radicals and hence trigger polymerization. However, because we are illuminating the GNRs off-resonance, the structures are not expected to absorb any significant light, and hence, the local temperature increase is expected to be negligible. Additionally, we believe that the effect of local heating of the GNR will be homogeneous and will not depend on the incident polarization.[24] This implies that thermal polymerization, if any, will be induced at every single point of the metal structure regardless of the unit normal vector direction with respect to the incident field polarization.

In conclusion, we have reported on nanoscale photopolymerization on the surface of nonresonant metal nanostructures. The photopolymerization is triggered by the localized electromagnetic field enhancement associated with the surface charge densities supported by the nanorod edges. The controlled photopolymerization at the nanometric scale relies on overcoming the threshold dose of the photosensitive formulation; judging by the high density of charge excited by the normal components of the electric field at the interface of the metal/dielectric, we demonstrated that the effective dose at some precise positions overcomes the threshold dose of the photopolymer, and hence, the polymerization process is initiated. To the best of our knowledge, this is the first time that the signature of the spatial distribution of the surface charges has been visualized.

This also demonstrates the versatility of the photochemical imaging approach, which is sensitive enough to imprint nonresonant fields.

AUTHOR INFORMATION

Corresponding Author:

*To whom correspondence should be addressed. E-mail: renaud.bachelot@utt.fr.

ACKNOWLEDGMENT The authors thank the Agence Nationale de la Recherche (ANR), under Grant Photohybrid (BLANC 07-2-188654). P.J. acknowledges UCB Miller Institute funds. The authors would like also to thank Dr. F. Charra for fruitful discussions.

REFERENCES

(1) Orfanidis, S. J. *Electromagnetic Waves and Antennas*; Sophocles Orfanidis (copyright holder): Piscataway, NJ, 2008.

(2) Alvarez-Puebla, R. A.; Liz-Marzan, L. M.; de Abajo, J. G.; Light, F. Concentration at the Nanometer Scale. *J. Phys. Chem. Lett.* **2010,** *1*, 2428–2434.

DOI: 10.1021/jz1014696 | *J. Phys. Chem. Lett.* **2011**, *2*, 7–11

(3) Clarke, M. L.; Grace Chou, S.; Hwang, J. Monitoring Photothermally Excited Nanoparticles via Multimodal Microscopy. *J. Phys. Chem. Lett.* **2010,** *1*, 1743–1748.
(4) Achermann, M. Exciton−Plasmon Interactions in Metal−Semiconductor Nanostructures. *J. Phys. Chem. Lett.* **2010,** *1*, 2837–2843.
(5) Nabika, H.; Takase, M.; Nagasawa, F.; Murakoshi, K. Toward Plasmon-Induced Photoexcitation of Molecules. *J. Phys. Chem. Lett.* **2010,** *1*, 2470–2487.
(6) Atwater, H. A.; Polman, A. Plasmonics for Improved Photovoltaic Devices. *Nat. Mater.* **2010,** *9*, 205–213.
(7) Juan, M. L.; Gordon, R.; Pang, Y.; Eftekhari, F.; Quidant, R. Self-Induced Back-Action Optical Trapping of Dielectric Nanoparticles. *Nat. Phys.* **2009,** *5*, 915–919.
(8) Eghlidi, H.; Lee, K. G.; Chen, X. W.; Götzinger, S.; Sandoghdar, V. Resolution and Enhancement in Nanoantenna-Based Fluorescence Microscopy. *Nano Lett.* **2009,** *9*, 4007–4011.
(9) Bergman, D. J.; Stockman, M. I. Surface Plasmon Amplification by Stimulated Emission of Radiation: Quantum Generation of Coherent Surface Plasmons in Nanosystems. *Phys. Rev. Lett.* **2003,** *90*, 027402.
(10) Noginov, M. A.; Zhu, G.; Belgrave, A. M.; Bakker, R.; Shalaev, V. M.; Narimanov, E. E.; Stout, S.; Herz, E.; Suteewong, T.; Wiesner, U. Demonstration of a Spaser-Based Nanolaser. *Nature* **2009,** *460*, 1110–1113.
(11) Douillard, L.; Charra, F.; Korczak, Z.; Bachelot, R.; Kostcheev, S.; Lerondel, G.; Adam, P. M.; Royer, P. Short Range Plasmon Resonators Probed by Photoemission Electron Microscopy. *Nano Lett.* **2008,** *8*, 935–940.
(12) Anker, J. N.; Hall, W. P.; Lyandres, O.; Shah, N. C.; Zhao, J.; Van Duyne, R. P. Biosensing with Plasmonic Nanosensors. *Nat. Mater.* **2008,** *7*, 442–453.
(13) Gersten, J. I. The Effect of Surface Roughness on Surface Enhanced Raman Scattering. *J. Chem. Phys.* **1980,** *72*, 5779–5780.
(14) Mohamed, M. B.; Volkov, V.; Link, S.; El-Sayed, M. A. The Lightning Gold Nanorods: Fluorescence Enhancement of Over a Million Compared to the Gold Metal. *J. Chem. Phys. Lett.* **2000,** *317*, 517–523.
(15) Bachelot, R.; H'dhili, F.; Barchiesi, D.; Lerondel, G.; Fikri, R.; Royer, P.; Landraud, N.; Peretti, J.; Chaput, F.; Lampel, G.; et al. Apertureless Near-Field Optical Microscopy: A Study of the Local Tip Field Enhancement Using Photosensitive Azobenzene-Containing Films. *J. Appl. Phys.* **2003,** *94*, 2060–2073.
(16) Van Bladel, J. *Singular Electromagnetic Fields and Sources*; Wiley-IEEE Press: New York, 2002.
(17) Lamprecht, B.; Krenn, J. R.; Leitner, A.; Aussenegg, F. R. Resonant and Off-Resonant Light-Driven Plasmons in Metal Nanoparticles Studied by Femtosecond-Resolution Third-Harmonic Generation. *Phys. Rev. Lett.* **1999,** *83*, 4421.
(18) Scharte, M.; Porath, R.; Ohms, T.; Aeschlimann, M.; Krenn, J. R.; Ditlbacher, H.; Aussenegg, F. R.; Liebsch, A. Do Mie Plasmons Have a Longer Lifetime on Resonance Than Off-Resonance? *Appl. Phys. B: Laser Opt.* **2001,** *73*, 305–310.
(19) Ibn El Ahrach, H.; Bachelot, R.; Vial, A.; Lerondel, G.; Plain, J.; Royer, P.; Soppera, O. Spectral Degeneracy Breaking of the Plasmon Resonance of Single Metal Nanoparticles by Nanoscale Near-Field Photopolymerization. *Phys. Rev. Lett.* **2007,** *98*, 107402.
(20) Deeb, C.; Bachelot, R.; Plain, J.; Baudrion, A. L.; Jradi, S.; Bouhelier, A.; Soppera, O.; Jain, P. K.; Huang, L.; Ecoffet, C.; et al. Quantitative Analysis of Localized Surface Plasmons Based on Molecular Probing. *ACS Nano* **2010,** *4*, 4579–4586.
(21) Draine, B. T.; Flatau, P. J. Discrete-Dipole Approximation for Scattering Calculations. *J. Opt. Soc. Am. A* **1994,** *11*, 1491–1499.
(22) Johnson, P. B.; Christy, R. W. Optical Constants of the Noble Metals. *Phys. Rev. B.* **1972,** *6*, 4370–4379.
(23) EM Explorer 2.0. http://www.emexplorer.net (2010).
(24) Govorov, A. O.; Richardson, H. H. Generating Heat With Metal Nanoparticles. *Nano Today* **2007,** *2*, 30–38.

DOI: 10.1021/jz1014696 | *J. Phys. Chem. Lett.* **2011,** *2*, 7–11